ELSEVIER

International Journal of Solids and Structures 41 (2004) 1945–1959

INTERNATIONAL JOURNAL OF SOLIDS and STRUCTURES

www.elsevier.com/locate/ijsolstr

Hertzian contact of orthotropic materials

Stephen R. Swanson *

Department of Mechanical Engineering, University of Utah, 50 S. Central Campus Drive, Salt Lake City, UT 84112, USA

Received 15 March 2003

Abstract

Contact loading of orthotropic materials is of interest in impact problems and other applications with composite materials. Although solutions are available for special cases such as transversely isotropic materials, solutions for contact loading for more general orthotropic materials have appeared much less frequently in the literature. The present work shows that a general procedure for calculating stresses due to contact loading can be obtained by combining two previous solution techniques. The first is the procedure outlined by Willis, that uses numerical contour integration to determine the size and aspect ratio of the elliptical contact area, and the contact pressure distribution. Detailed stress fields are then obtained by using these parameters in the general solution for transverse pressure loading of laminated orthotropic materials due to Pagano and Srinivas and Rao. Comparisons with known results for special cases, along with comparisons of surface displacements and the indentor profile, indicate that good accuracy of the solution can be achieved.

Keywords: Hertzian contact; Contact stress; Contact loading; Orthotropic materials

1. Introduction

Hertzian contact of orthotropic materials is of interest in a number of applications, including those associated with foreign body impact in composite materials. Contact loading poses a mixed boundary value problem, as displacements are specified inside the loading area and tractions outside, and further the size and shape of the contact zone are initially unknown and are part of the solution. A variety of solutions are available and have been summarized by Johnson (1985), for various problems which include such complicating factors as friction in the contact zone. However solutions for non-isotropic materials are much less available. Work on contact loading of transversely isotropic materials has been presented by Green and Zerna (1954), Leknitskii (1963), Sveklo (1964), Dahan and Zarka (1977), and in a particularly convenient form by Turner (1966). A numerical approach to the contact problem for orthotropic materials has been recently presented by Shi et al. (2003). A procedure for determining some of the features of the contact

* Tel.: +1-801-581-6407; fax: +1-801-585-9826.
E-mail address: swanson@mech.utah.edu (S.R. Swanson).

0020-7683/$ - see front matter © 2003 Elsevier Ltd. All rights reserved.
doi:10.1016/j.ijsolstr.2003.11.003

problem for generally anisotropic materials has been given by Willis (1966), that involves numerical contour integration.

It has been widely appreciated that if the contact loading zone size and shape, and the pressure distribution over the contact zone were known, the details of the contact stresses could be investigated with simpler solutions of problems with entirely stress-prescribed boundary conditions. One such solution that is available for transverse pressure loading of orthotropic materials is that due to Pagano (1970) and Srinivas and Rao (1970). This solution is given in terms of Fourier series expansions of transverse pressure loading on layered orthotropic materials with simply supported edges. By selecting suitable geometries, this solution can be readily adapted to determining stresses in orthotropic materials, once the contact zone and pressure have been determined.

Some approximate procedures have been utilized to obtain insight into contact loading of orthotropic materials. Yang and Sun (1982) and Tan and Sun (1985) assumed that the contact pressure and contact area could be obtained from the usual formulas for isotropic materials, but with the isotropic modulus of elasticity replaced by the orthotropic modulus in the loading direction. Wu and Yen (1994) and Chao and Tu (1999) have used the Pagano solution as a Green's function approximating a point load, and then numerically associated the resulting surface displacements to the indentor geometry. However it is difficult to assess the resulting accuracy.

The 2-D problem of contact of a plane stress or plane strain strip by a cylindrical roller is simpler than the 3-D problem, and a solution for general anisotropic materials has been presented by Miller (1986) and Chen (1969).

No results have appeared in the literature that utilize the approach outlined by Willis (1966), possibly because it appears difficult to obtain the full solution from this method. However, in the following it will be shown that the procedure of Willis can be readily applied to determine the contact area and pressure distribution for orthotropic materials, which can then be combined with the Pagano solution to determine as much information about the resulting stress and strain fields as desired. Results will be given for orthotropic materials, as well as for the simpler case of transversely isotropic materials to assess accuracy.

2. Point loading of an anisotropic half-space

Willis (1966) first develops the solution for point loading of an anisotropic half-space. This solution will be briefly outlined in the following: Consider that the x_3 direction is normal to the surface of the half-space. The equilibrium equations are written as usual as

$$\sigma_{ij,j} = 0, \tag{1}$$

where a repeated subscript denotes a summation, and the comma denotes differentiation. The stress–strain law for a generally anisotropic material can be written as

$$\{\sigma\} = [C]\{\varepsilon\}, \tag{2}$$

where

$$\{\sigma\}^{\mathrm{T}} = \{\,\sigma_{11} \quad \sigma_{22} \quad \sigma_{33} \quad \sigma_{23} \quad \sigma_{31} \quad \sigma_{12}\,\},$$
$$\{\varepsilon\}^{\mathrm{T}} = \{\,\varepsilon_{11} \quad \varepsilon_{22} \quad \varepsilon_{33} \quad 2\varepsilon_{23} \quad 2\varepsilon_{31} \quad 2\varepsilon_{12}\,\}.$$

The stress–strain relationship for orthotropic materials reduces to

$$\begin{Bmatrix}\sigma_{11}\\ \sigma_{22}\\ \sigma_{33}\end{Bmatrix} = \begin{bmatrix}C_{11} & C_{12} & C_{13}\\ C_{21} & C_{22} & C_{23}\\ C_{31} & C_{32} & C_{33}\end{bmatrix}\begin{Bmatrix}\varepsilon_{11}\\ \varepsilon_{22}\\ \varepsilon_{33}\end{Bmatrix} \quad \text{and} \quad \begin{Bmatrix}\sigma_{23}\\ \sigma_{31}\\ \sigma_{12}\end{Bmatrix} = \begin{bmatrix}C_{44} & 0 & 0\\ 0 & C_{55} & 0\\ 0 & 0 & C_{66}\end{bmatrix}\begin{Bmatrix}2\varepsilon_{23}\\ 2\varepsilon_{31}\\ 2\varepsilon_{12}\end{Bmatrix}. \tag{3}$$

The strains are related to the displacements through the usual strain–displacement relationship:

$$\varepsilon_{ij} = \frac{1}{2}(u_{i,j} + u_{j,i}). \tag{4}$$

Substituting the stress–strain and strain–displacement relations into the equations of equilibrium gives the following: The case of an orthotropic material given by Eq. (3) will be displayed, although Willis retains the general form of an anisotropic material of Eq. (2). The resulting field equations are

$$\begin{aligned}
&C_{11}u_{1,11} + C_{66}u_{1,22} + C_{55}u_{1,33} + (C_{12} + C_{66})u_{2,12} + (C_{13} + C_{55})u_{3,13} = 0,\\
&C_{22}u_{2,22} + C_{66}u_{2,11} + C_{44}u_{2,33} + (C_{12} + C_{66})u_{1,12} + (C_{23} + C_{44})u_{3,23} = 0,\\
&C_{33}u_{3,33} + C_{55}u_{3,11} + C_{44}u_{3,22} + (C_{13} + C_{55})u_{1,12} + (C_{23} + C_{44})u_{2,23} = 0.
\end{aligned} \tag{5}$$

Define the Fourier transform as

$$\tilde{f}(\xi_1) \equiv \frac{1}{\sqrt{2\pi}} \int_{-\infty}^{\infty} f(x_1)\exp(\mathrm{i}\xi_1 x_1)\,\mathrm{d}x_1 \tag{6}$$

and taking Fourier transforms of Eqs. (5) with respect to x_1 and x_2 gives

$$\begin{aligned}
&(C_{11}\xi_1^2 + C_{66}\xi_2^2)\tilde{u}_1 - C_{55}\tilde{u}_{1,33} + \xi_1\xi_2(C_{12} + C_{66})\tilde{u}_2 + \mathrm{i}\xi_1(C_{13} + C_{55})\tilde{u}_{3,3} = 0,\\
&\xi_1\xi_2(C_{12} + C_{66})\tilde{u}_1 + (C_{66}\xi_1^2 + C_{22}\xi_2^2)\tilde{u}_2 - C_{44}\tilde{u}_{2,33} + \mathrm{i}\xi_2(C_{23} + C_{44})\tilde{u}_{3,3} = 0,\\
&\mathrm{i}\xi_1(C_{13} + C_{55})\tilde{u}_{1,3} + \mathrm{i}\xi_2(C_{23} + C_{44})\tilde{u}_{2.3} + (C_{55}\xi_1^2 + C_{44}\xi_2^2)\tilde{u}_3 - C_{33}\tilde{u}_{3,33} = 0.
\end{aligned} \tag{7}$$

Now assume the solution in the form

$$\begin{Bmatrix} \tilde{u}_1 \\ \tilde{u}_2 \\ \tilde{u}_3 \end{Bmatrix} = \begin{Bmatrix} A_1 \\ A_2 \\ A_3 \end{Bmatrix} \exp(\mathrm{i}mx_3). \tag{8}$$

Substituting (8) into (7) gives

$$\begin{bmatrix} m^2 + \frac{C_{11}}{C_{55}}\xi_1^2 + \frac{C_{66}}{C_{55}}\xi_2^2 & \frac{C_{12}+C_{66}}{C_{55}}\xi_1\xi_2 & -m\frac{C_{13}+C_{55}}{C_{55}}\xi_1 \\ & m^2 + \frac{C_{66}}{C_{44}}\xi_1^2 + \frac{C_{22}}{C_{44}}\xi_2^2 & -m\frac{C_{23}+C_{44}}{C_{44}}\xi_2 \\ \text{sym} & & m^2 + \frac{C_{55}}{C_{33}}\xi_1^2 + \frac{C_{44}}{C_{33}}\xi_2^2 \end{bmatrix} \begin{Bmatrix} A_1 \\ A_2 \\ A_3 \end{Bmatrix} = \begin{Bmatrix} 0 \\ 0 \\ 0 \end{Bmatrix}. \tag{9}$$

Redefining the material constants as

$$\begin{aligned}
&b_1 = \frac{C_{11}}{C_{55}}, \quad b_2 = \frac{C_{66}}{C_{55}}, \quad b_3 = \frac{C_{66}}{C_{44}}, \quad b_4 = \frac{C_{22}}{C_{44}}, \quad b_5 = \frac{C_{55}}{C_{33}},\\
&b_6 = \frac{C_{44}}{C_{33}}, \quad b_7 = \frac{C_{12} + C_{66}}{C_{55}}, \quad b_8 = \frac{C_{13} + C_{55}}{C_{55}}, \quad b_9 = \frac{C_{23} + C_{44}}{C_{44}}
\end{aligned} \tag{10}$$

and further defining

$$\begin{aligned}
&e_1 = b_1 + b_3 + b_5 - b_8^2, \quad e_2 = b_2 + b_4 + b_6 - b_9^2, \quad e_3 = b_1b_3 + b_1b_5 + b_3b_5 - b_3b_8^2,\\
&e_4 = b_2b_3 + b_1b_4 + b_2b_5 + b_4b_5 + b_1b_6 + b_3b_6 + 2b_7b_8b_9 - (b_4b_8^2 + b_1b_9^2 + b_7^2),\\
&e_5 = b_2b_4 + b_2b_6 + b_4b_6 - b_2b_9^2, \quad e_6 = b_1b_3b_5, \quad e_7 = b_2b_3b_5 + b_1b_4b_5 + b_1b_3b_6 - b_5b_7^2,\\
&e_8 = b_2b_4b_5 + b_2b_3b_6 + b_1b_4b_6 - b_6b_7^2, \quad e_9 = b_2b_4b_6
\end{aligned} \tag{11}$$

and setting the determinant of the coefficient matrix to zero gives a cubic equation in m^2 as

$$m^6 + (e_1\xi_1^2 + e_2\xi_2^2)m^4 + (e_3\xi_1^4 + e_4\xi_1^2\xi_2^2 + e_5\xi_2^4)m^2 + (e_6\xi_1^6 + e_7\xi_1^4\xi_2^2 + e_8\xi_1^2\xi_2^4 + e_9\xi_2^6) = 0. \tag{12}$$

This equation has three roots for m^2 and six roots for m given by

$$m_k = \pm\sqrt{\alpha_j^2}, \quad j = 1:3 \;\; k = 1:6. \tag{13}$$

Substituting these roots back into the first two equations of (9) gives the ratio of the coefficients from

$$\begin{bmatrix} m^2 + b_1\xi_1^2 + b_2\xi_2^2 & b_7\xi_1\xi_2 \\ b_7\xi_1\xi_2 & m^2 + b_3\xi_1^2 + b_4\xi_2^2 \end{bmatrix} \begin{Bmatrix} A_1/A_3 \\ A_2/A_3 \end{Bmatrix} = \begin{Bmatrix} mb_8\xi_1 \\ mb_9\xi_2 \end{Bmatrix} \tag{14}$$

with the resulting transformed displacements given as

$$\begin{Bmatrix} \tilde{u}_1 \\ \tilde{u}_2 \\ \tilde{u}_3 \end{Bmatrix} = \sum_{k=1}^{6} \begin{Bmatrix} (A_1/A_3)_k \\ (A_2/A_3)_k \\ 1 \end{Bmatrix} A_{3_k} \exp(\mathrm{i}m_k(\xi_1, \xi_2)x_3). \tag{15}$$

The six constants are determined from the boundary conditions for a point load on a half-space. The condition that the displacements be finite far from the load indicates that only the roots with positive imaginary parts be retained. The remaining three constants are determined from the stress boundary conditions on the surface, which are

$$\sigma_{13}(x_1, x_2, 0) = 0, \quad \sigma_{23}(x_1, x_2, 0) = 0, \quad \sigma_{33}(x_1, x_2, 0) = -\delta(x_1)\delta(x_2). \tag{16}$$

Substituting the stress–strain and strain–displacement relations, and taking Fourier transforms gives the following equations:

$$\begin{aligned} &\sum_{k=1}^{3} [m_k(A_1/A_3)_k - \xi_1]A_{3_k} = 0, \\ &\sum_{k=1}^{3} [m_k(A_2/A_3)_k - \xi_2]A_{3_k} = 0, \\ &\sum_{k=1}^{3} [C_{13}\xi_1(A_1/A_3)_k + C_{23}\xi_2(A_2/A_3)_k - C_{33}m_k]A_{3_k} = \frac{-\mathrm{i}}{2\pi}. \end{aligned} \tag{17}$$

The remaining three constants are determined from Eqs. (17), and thus the solution is obtained for the Fourier transformed displacements, for the problem of a point load on an orthotropic half-space, in terms of the transform parameters ξ_1 and ξ_2.

3. Solution of the contact problem

The above solution for the displacements due to a unit point load is integrated over the contact area and contact pressure to obtain the displacements due to the contact loading, and then matched to the indentor geometry. Willis conditionally assumes, and subsequently proves, that the contact area is an ellipse with dimensions $2a_1 \times 2a_2$, with values to be determined subsequently, and that the pressure distribution is given by

$$p(x_1, x_2) = p_0\left(1 - \frac{x_1^2}{a_1^2} - \frac{x_2^2}{a_2^2}\right)^{1/2}. \tag{18}$$

The surface displacement is then given by

$$u_3(x_1, x_2, 0) = \int_S \int p_0\left(1 - \frac{x_1'^2}{a_1^2} - \frac{x_2'^2}{a_2^2}\right)^{1/2} w(x_1 - x_1', x_2 - x_2')\,\mathrm{d}x_1'\,\mathrm{d}x_2', \tag{19}$$

where S denotes the contact area, and the surface displacement due to the point load is denoted as w, as

$$w(x_1, x_2) \equiv u_3(x_1, x_2, 0). \tag{20}$$

While w has not been found explicitly, its Fourier transform is given in Eq. (15). Substituting the inverse Fourier transform of the surface displacement into (19) gives

$$u_3(x_1, x_2, 0) = \int_S \int p_0 \left(1 - \frac{x_1'^2}{a_1^2} - \frac{x_2'^2}{a_2^2}\right)^{1/2} \frac{1}{2\pi} \int_{-\infty}^{\infty} \int_{-\infty}^{\infty} \tilde{w}(\xi_1, \xi_2) \exp[-\mathrm{i}(\xi_1(x_1 - x_1') + \xi_2(x_2 - x_2'))] \, \mathrm{d}\xi_1 \, \mathrm{d}\xi_2 \, \mathrm{d}x_1' \, \mathrm{d}x_2'. \tag{21}$$

Willis reduces the above to a single line integral that can be carried out with numerical integration. The integral becomes

$$u_3(x_1, x_2, 0) = p_0 \frac{\pi a_2}{4} \int_0^{2\pi} \tilde{w}(\varepsilon\eta_1, \eta_2) \left\{1 - \left(\frac{\eta_1 x_1}{a_1} + \frac{\eta_2 x_2}{a_2}\right)^2\right\} \mathrm{d}\theta, \tag{22}$$

where

$$\varepsilon \equiv \frac{a_2}{a_1}, \quad \eta_1 = \cos\theta, \quad \eta_2 = \sin\theta. \tag{23}$$

The contact force is related to the peak contact pressure by

$$F = \frac{2}{3} p_0 \pi a_1 a_2. \tag{24}$$

The relative displacement of the indentor and half-space can be expressed in the form

$$w_I + w_{hs} = \alpha - (Ax_1^2 + Bx_2^2 + 2Hx_1x_2). \tag{25}$$

In the special case of a rigid indentor

$$A = \frac{1}{2R_1}, \quad B = \frac{1}{2R_2} \tag{26}$$

and for an orthotropic material, where the axis of the elliptical contact area is aligned with the axes of orthotropy,

$$\frac{1}{2R_1} = \frac{3FI_1}{8a_1^3}, \quad \frac{1}{2R_2} = \frac{3FI_2}{8a_1a_2^2}, \quad \delta = \frac{3FI_3}{8a_1} = \left(\frac{3F}{4\sqrt{R_1}}\right)^{2/3} \left(\frac{I_3}{2I_1^{1/3}}\right), \tag{27}$$

where

$$I_1 = \int_0^{2\pi} \tilde{w}(\varepsilon\eta_1, \eta_2)\eta_1^2 \, \mathrm{d}\theta, \quad I_2 = \int_0^{2\pi} \tilde{w}(\varepsilon\eta_1, \eta_2)\eta_2^2 \, \mathrm{d}\theta, \quad I_3 = \int_0^{2\pi} \tilde{w}(\varepsilon\eta_1, \eta_2) \, \mathrm{d}\theta. \tag{28}$$

From (27), it can be seen that

$$\frac{I_2}{I_1} = \frac{a_2^2}{a_1^2} \frac{R_1}{R_2} = \varepsilon^2 \frac{R_1}{R_2}. \tag{29}$$

Solving for a_1, a_2, and δ for a rigid spherical indentor gives

$$a_1 = \left(\frac{3RF}{4}\right)^{1/3} I_1^{1/3}, \quad a_2 = \left(\frac{3RF}{4}\right)^{1/3} \frac{I_2^{1/2}}{I_1^{1/6}}, \quad \delta = \left(\frac{3F}{4\sqrt{R}}\right)^{2/3} \frac{I_3}{2I_1^{1/3}}. \tag{30}$$

The solution algorithm for contact loading of an orthotropic half-space can then be written as follows:

Step 1. Select a starting value for ε (say $\varepsilon = 1$).
Step 2. Compute the integrals I_1 and I_2 of Eq. (28).

The integrals are computed by incrementing θ, using $\eta_1 = \cos\theta$ and $\eta_2 = \sin\theta$. Then set $\xi_1 = \varepsilon\cos\theta$ and $\xi_2 = \sin\theta$. Compute the roots and solve for the coefficients A_{3k} from Eq. (17). This gives

$$\tilde{w}(\varepsilon\eta_1, \eta_2) = \sum_{k=1}^{3} A_{3k}. \tag{31}$$

The integrals are then determined by numerically integrating these functions to get I_1 and I_2.

Step 3. A new value of ε is determined from Eq. (29). This value can then be used in step 1, and steps 1–3 repeated until the solution for ε converges. This can be considered as a root finding problem for ε. Any root finding algorithm (the simple bisection method was used here) can be employed.
Step 4. Once a converged value of ε is obtained, the complete solution can be obtained by computing I_3, and using Eq. (30) to determine the size of the contact zone and the depth of the indentation for a given contact force.

4. Illustration of determining contact parameters

4.1. Cubic media

Willis (1966) presents results for a special class of orthotropic materials, termed cubic media. This class of materials has three independent material constants, and the stress–strain relationship is given by

$$\begin{Bmatrix} \sigma_{11} \\ \sigma_{22} \\ \sigma_{33} \end{Bmatrix} = \begin{bmatrix} \lambda+2\mu' & \lambda & \lambda \\ \lambda & \lambda+2\mu' & \lambda \\ \lambda & \lambda & \lambda+2\mu' \end{bmatrix} \begin{Bmatrix} \varepsilon_{11} \\ \varepsilon_{22} \\ \varepsilon_{33} \end{Bmatrix} \quad \text{and} \quad \begin{Bmatrix} \sigma_{23} \\ \sigma_{31} \\ \sigma_{12} \end{Bmatrix} = \begin{bmatrix} \mu & 0 & 0 \\ 0 & \mu & 0 \\ 0 & 0 & \mu \end{bmatrix} \begin{Bmatrix} 2\varepsilon_{23} \\ 2\varepsilon_{31} \\ 2\varepsilon_{12} \end{Bmatrix}. \tag{32}$$

Because of the symmetry of the material properties, the contact area is a circle and $\varepsilon = 1$. As a specific example, the computations above were carried out for values of $E = 70$ GPa, $\nu = 0.3$ and $\mu/\mu' = 8$. Thus $\lambda = \nu E/(1+\nu)(1-2\nu) = 40.38$ GPa, $\mu' = E/2(1+\nu) = 26.92$ GPa, and $\mu = 215.38$ GPa. Plots of the functions f_1, f_2, and f_3 (normalized by multiplying by $E_{33} = E$) that are the integrands of I_1, I_2, and I_3, respectively, are shown in Fig. 1. The values of the integrals are $I_1 = I_2 = 7.117E-3$ GPa^{-1}, and $I_3 = 1.423E-2$ GPa^{-1}. These results agree with those presented by Willis (1966).

4.2. Transversely isotropic materials

Solutions for contact problems with transversely isotropic materials have been presented by a number of authors, and thus offer an opportunity to compare with the present contour integration approach. A general solution has been presented by Turner (1966), who shows that the contact zone and size can be found from formulas similar to those for isotropic contact problems, if the isotropic modulus is replaced by a combination of the transversely isotropic properties. Thus for normal contact

$$a = \left(\frac{3RF}{4E^*_{TI}}\right)^{1/3} \quad \text{and} \quad \delta = \left(\frac{3F}{4\sqrt{R}E^*_{TI}}\right)^{2/3}. \tag{33}$$

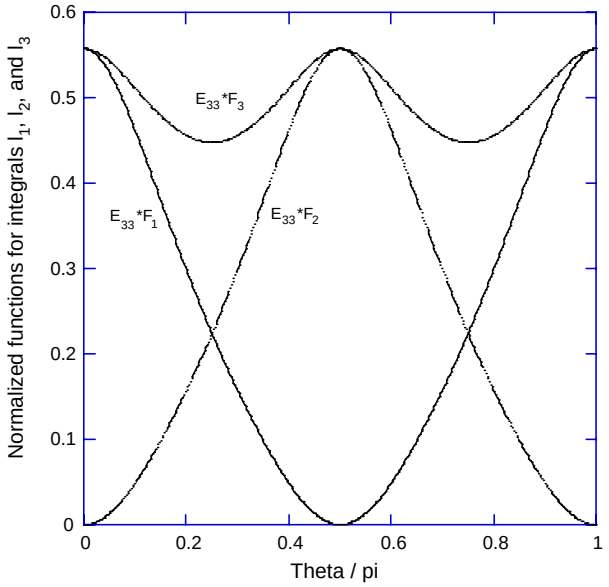

Fig. 1. Functions used in numerical contour integration for contact loading of a cubic media orthotropic material.

Turner defines the effective modulus as follows: Let

$$\alpha = \left(\frac{E_x/E_z - \nu_{xz}^2}{1 - \nu_{xy}^2} \right)^{1/2} \quad \text{and} \quad \beta = \frac{1 + \left(\frac{E_x}{2G_{xz}} - 1 \right) - \nu_{xz}(1 + \nu_{xy})}{1 - \nu_{xy}^2}, \tag{34}$$

then

$$E_{TI}^* = \left(\frac{2}{\alpha\beta} \right). \tag{35}$$

This effective modulus for transversely isotropic normal contact reduces to $E/(1-\nu^2)$ for isotropic materials. As a specific example, values of $E_x = 51.3$ GPa, $\nu_{xy} = 0.292$, $E_z = 12$ GPa, $\nu_{xz} = 0.28$, and $G_{xz} = 6$ GPa were used. These values correspond to a transversely isotropic laminate of AS4 carbon fiber and epoxy (Swanson, 1997). The resulting value from Eq. (35) is $E_{ti}^* = 14.61$ GPa.

Comparable results can also can be calculated using contour integration as described above. However, the first two equations of (17) are not independent. Letting the material properties approach the transversely isotropic case shows that the coefficient corresponding to the middle root approaches zero. Thus only the first and third of Eq. (17) need be used, to solve for the two remaining coefficients. Comparing Eqs. (27) and (33) shows that

$$E_{TI}^* = \left(\frac{2I_1^{1/3}}{I_3} \right)^{3/2}. \tag{36}$$

The functions for the integrals for this case are shown in Fig. 2, normalized as before by multiplying by E_{33}. The numerical integration of these functions gives $I_1 = I_2 = 6.843E-2$, $I_3 = 0.1369$ GPa^{-1}. Using Eqs. (27) and (33), it can be seen that these values agree with Eq. (35), and thus the Turner and Willis numerical contour integration results are in agreement.

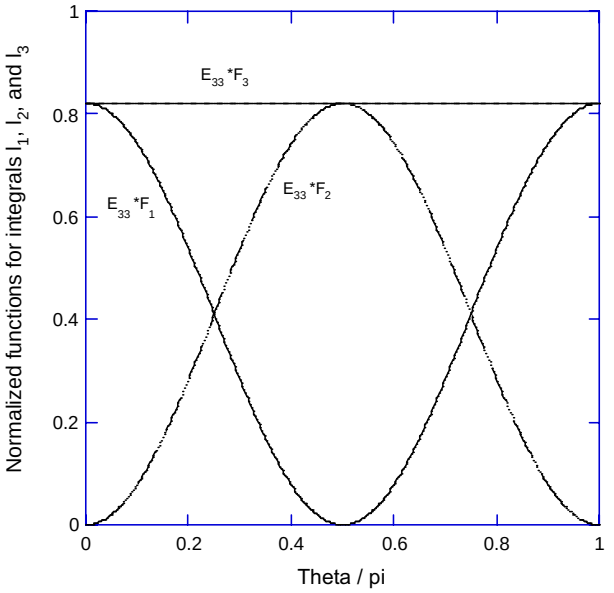

Fig. 2. Functions used in numerical contour integration for contact loading of a transversely isotropic material.

The transversely isotropic material is a special case, and can be solved using the Willis approach without using numerical integration. The simplification of the material properties permits Eq. (12) to be written as

$$m^6 + e_1(\xi_1^2 + \xi_2^2)m^4 + e_3(\xi_1^2 + \xi_2^2)^2 m^2 + e_6(\xi_1^2 + \xi_2^2)^3 = 0 \tag{37}$$

permitting m to be solved for explicitly and the rest of the computation can then be carried out analytically, as shown by Willis (1966). This approach then leads to the same answers as above.

Yang and Sun (1982) and Tan and Sun (1985) have proposed an approximation for the contact deformation, by using the second of Eq. (33) with E^* simply replaced by E_z. The accuracy of this approximation can be checked for transversely isotropic materials by comparing with the exact results given here. The results of this comparison are shown in Fig. 3. Here the transversely isotropic material properties used above are modified so that E_z, G_{xz}, and v_{xz} are all modified so that they uniformly approach an isotropic material. Since the effective modulus of Eq. (35) depends on all of the properties and not just E_z, the approximation of Sun et al. holds exactly only for the isotropic case, and decreases in accuracy as E_z differs from E_x. This can be seen in Fig. 3. The error of the Sun et al. approximation is on the order of 22% for material properties typical of carbon fiber laminates.

4.3. General orthotropic material

The results given above are similar to those available in the literature, and have served primarily to establish that the method is working properly. However the numerical contour integration procedure as outlined above can be used to calculate the parameters of the contact problem for more general orthotropic materials, and results of this type have not previously appeared in the literature.

The orthotropic material considered in the following is made up of a "well dispersed" laminate consisting of various numbers of 0 and 90° plies of a carbon/epoxy material. The properties of a unidirectional lamina are given in Table 1. Orthotropic properties are then calculated for other layups using standard lamination theory. In all cases, the properties are then averaged through the thickness so that a single

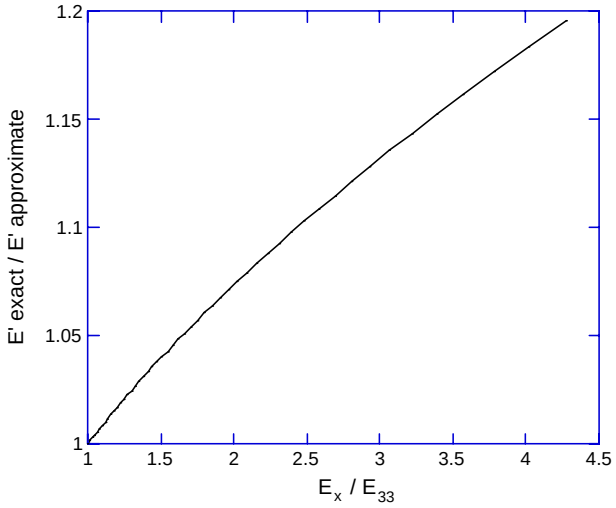

Fig. 3. Ratio of exact effective modulus to the approximation of Sun et al. for contact indentation of a transversely isotropic material.

Table 1
Material properties of an orthotropic lamina used in contact loading

Property	Value	Property	Value
E_{11}	127 GPa	E_{33}	12 GPa
E_{22}	11 GPa	G_{13}	6 GPa
G_{12}	6.55 GPa	G_{23}	6 GPa
ν_{12}	0.28	ν_{13}	0.28
		ν_{23}	0.28

equivalent orthotropic material is being considered. As an example, consider that of an orthotropic material equivalent to a unidirectional lamina, with the x axis taken in the fiber direction or the 1, 1 direction of Table 1. Following the procedure described above gives a final converged value of $\varepsilon = 1.069$. The functions f_1, f_2, and f_3 for this value of ε are shown in Fig. 4, and the resulting numerical integrations give values of $I_1 = 6.338E-2$, $I_2 = 7.250E-2$, and $I_3 = 0.1359$ GPa^{-1}. Substituting these values into Eq. (30) gives the contact size and center indentation for a given contact force. It is interesting to note that even with properties as directional as used in this example, with $E_x/E_y = 11.5$, the difference between the major and minor axes of the elliptical contact area is about 7%.

Further calculations were performed using orthotropic properties obtained from lamination theory as described above. The results from these calculations are shown in Fig. 5. Fig. 5 shows the ratio of the axes of the elliptical contact area, a_2/a_1, as a function of the ratio of the in-plane moduli. Fig. 5 also shows two additional parameters related to the contact size and the deflection at the center of the contact area. Eq. (30) can be written as

$$a_1 = \left(\frac{3RF}{4}\right)^{1/3} I_1^{1/3} \quad \text{or} \quad a_1 = \left(\frac{3RF}{4E^*_{a1}}\right)^{1/3} \quad \text{with} \quad E^*_{a1} = \frac{1}{I_1}, \tag{38}$$

$$\delta = \left(\frac{3F}{4\sqrt{R}}\right)^{2/3} \frac{I_3}{2I_1^{1/3}} \quad \text{or} \quad \delta = \left(\frac{3F}{4\sqrt{R}E^*_{\delta}}\right)^{2/3} \quad \text{with} \quad E^*_{\delta} = \frac{I_1^{1/2}}{(I_3/2)^{3/2}}. \tag{39}$$

The values of the effective moduli in these two equations are also plotted in Fig. 5.

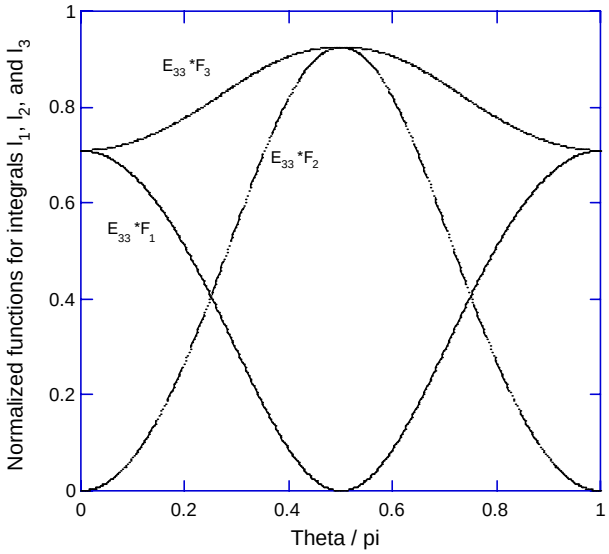

Fig. 4. Functions used in numerical contour integration for contact loading of an orthotropic material. The material has properties of a unidirectional fiber composite.

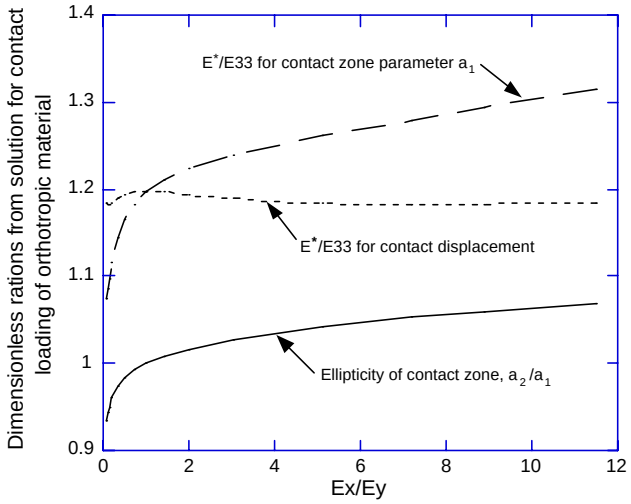

Fig. 5. Parameters of contact loading of orthotropic material from contour integration.

5. Stresses due to contact loading

Although some information on the stresses in the half-space due to the contact loading can be obtained from the contour integrals, it is simpler to just use the pressure distribution and size of the contact zone from the above, and then use the solution due to Pagano (1970) and Srinivas and Rao (1970), to obtain more detailed information. As mentioned above, this latter approach gives a complete solution for a

layered orthotropic material subject to arbitrary transverse pressure loading on the surface. The solution is general with respect to the number of the layers, the orthotropic material properties, and the thicknesses of the layers, but requires that the transverse displacement on the edges be zero, and that the normal stresses on the edges be zero. These conditions are considered to represent simply supported edges. By selecting a single layer that is large in the x and y directions and thick in the z direction with respect to the size of the contact area, the solution can be made to approximate transverse pressure loading of a half-space. The usual difficulty in applying this solution to contact problems is that the size and shape of the contact zone and pressure distribution are typically not known. However, as shown above, these parameters of contact loading of a half-space can readily be determined by using numerical contour integration.

The equations of the Pagano and Srinivas and Rao approach have been presented previously for the 3-D case in Swanson (2000), and have been used for contact problems in Wu and Yen (1994) and Chao and Tu (1999), and for 2-D contact in Swanson and Kim (2003). The details of the approach will not be repeated here, but one particular point will be made.

In the Pagano and Srinivas and Rao solution the displacements are obtained in terms of products of Fourier series in x and y and positive and negative exponentials in z, as

$$u_{mn}(x,y,z) = \left\{ \sum_{k=1}^{3} A_{kmn} \exp(s_k z) + \sum_{k=4}^{6} A_{kmn} \exp(-s_{k-3} z) \right\} \cos\frac{m\pi x}{a} \sin\frac{n\pi y}{b}. \tag{40}$$

The terms with positive exponentials give rise to numerical difficulties, and limit the number of terms that can be taken in the Fourier series. However, as shown for the 2-D case in Swanson and Kim (2003), this can be easily overcome by introducing a new length coordinate and redefining the constants, as follows: Let

$$\zeta = h - z, \tag{41}$$

where h is the thickness of the layer. Substituting in the terms with positive exponentials in z gives, for example,

$$A \exp(sz) = A \exp(s(h-\zeta)) = A \exp(sh) \exp(-s\zeta) = \overline{A} \exp(-s\zeta). \tag{42}$$

Using this new coordinate enables the solution to be written as

$$u_{mn}(x,y,z) = \left\{ \sum_{k=1}^{3} \overline{A}_{kmn} \exp(-s_k \zeta) + \sum_{k=4}^{6} A_{kmn} \exp(-s_{k-3} z) \right\} \cos\frac{m\pi x}{a} \sin\frac{n\pi y}{b}. \tag{43}$$

Thus only terms with negative exponentials enter the solution, and numerical problems associated with the positive exponentials are eliminated. The strains are obtained from derivatives of the displacements, noting that

$$\frac{\mathrm{d}}{\mathrm{d}z} = -\frac{\mathrm{d}}{\mathrm{d}\zeta}.$$

The stresses are related to the strains by the stress–strain law.

The above approach was then employed to determine the displacements, stresses, and strains throughout the orthotropic half-space for the contact problems previously considered. The first problem considered is that of a rigid spherical indentor contacting a transversely isotropic half-space. A contact radius of 1 mm was used for illustration, with the contact pressure distribution obtained from Eqs. (18), (24), and (30). This pressure distribution was then used as the transverse pressure loading. The geometry of the Pagano solution is that of a finite 3-D rectangular solid, but values of the lateral dimensions and thickness on the order of 50 times the contact radius removes the effect of the finite geometry. It is possible, and was done here, to apply the pressure distribution on both opposite faces of the solid so as to achieve an equivalent rigid boundary at

the midplane, from symmetry. Fitting of the Fourier series expansions of the pressure was accomplished using numerical Gauss integration of order 24 or 48.

A comparison of the surface displacements calculated in this way is shown in Fig. 6, along with the profile of the spherical indentor, using the material properties previously used for the transversely isotropic material of Fig. 2. It can be seen that the calculated displacement conforms closely with that of the indentor within the contact zone. Values for the root-mean-square deviation and the maximum deviation of surface displacement and indentor, normalized to the indentation depth, are on the order of 0.5% or less for typical calculations, using on the order of 100 terms in the Fourier series expansions. Thus this seems to be a very reasonable way to solve this contact problem. The Pagano solution can then be used to solve for all displacement, strain, and stress components of interest. For example, the normal strain in a radial direction along the top surface is shown calculated in Fig. 7. It can be seen that the strains are compressive in the contact zone, but change to tensile just outside the contact region.

The next problem considered was an orthotropic material, with properties that correspond to a fiber composite material with a $[0_{18}/90_2]$ layup, and averaged through the thickness to give $E_x = 116$ GPa, $E_y = 22.7$ GPa, $G_{xy} = 6.55$ GPa, and $v_{xy} = 0.136$. The through-the-thickness properties are given in Table 1 The elliptic contact zone and pressure loading obtained as shown in Figs. 4 and 5 along with Eqs. (18), (24), and (30) were used as input to the Pagano solution. The surface displacements calculated are shown in Fig. 8, along with the profile of the spherical indentor in both the x and y directions. Note that because of the orthotropic properties, the contact zone is elliptic, with a_2/a_1 equal to 1.042. It can be seen that the surface displacements calculated in the contact zone agree very well with the indentor profile, with values for the root-mean-square deviation and the maximum deviation of surface displacement and indentor, normalized to the indentation depth, again on the order of 0.5% or less for typical calculations. All stress and strain values are readily available, as in the previous problem. As an example, the loaded surface normal strains in the x and y directions are plotted vs x and y, respectively in Fig. 9. Since the problem is not symmetric, these normal strains are different from each other.

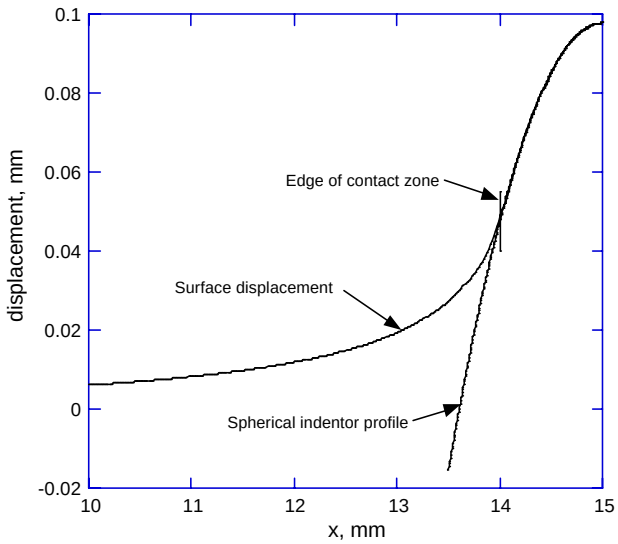

Fig. 6. Surface displacement determined from the Pagano solution in contact loading of a transversely isotropic material. Contact zone size and pressure distribution taken from Willis contour integration. Displacement is seen to match the indentor profile.

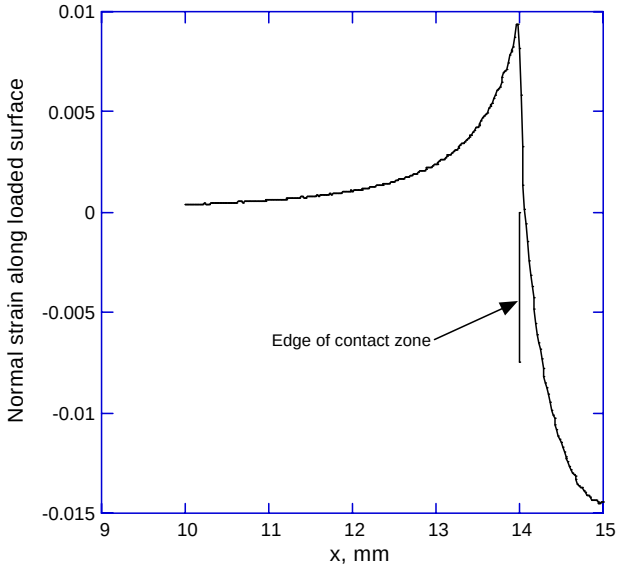

Fig. 7. Normal strain on loaded surface near the contact zone, calculated for a transversely isotropic material using the Pagano solution. Center of the contact zone is at $x = 15$ mm.

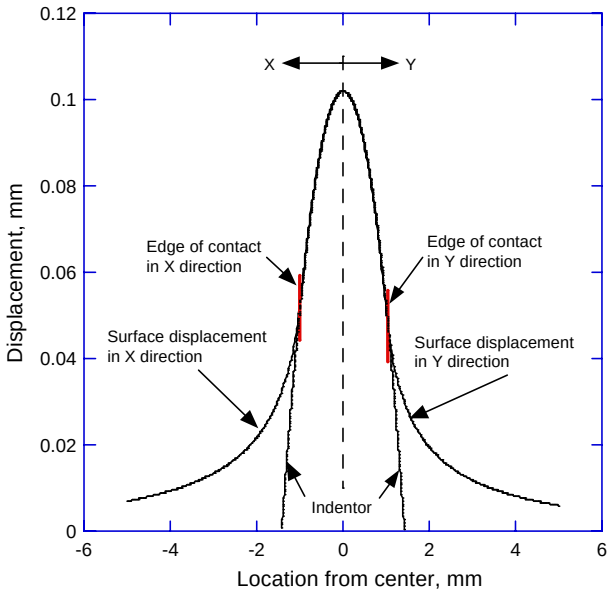

Fig. 8. Surface displacements determined from the Pagano solution in contact loading of an orthotropic material. Contact zone size and pressure distribution are taken from Willis contour integration. Displacement is seen to match the indentor profile in both the x and y directions, which are different because of the orthotropic material properties ($E_x/E_y = 5.10$, $a_2/a_1 = 1.042$).

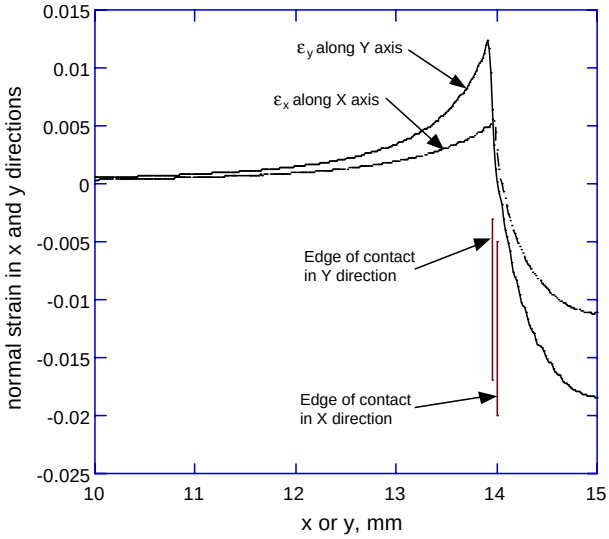

Fig. 9. Normal strain on loaded surface along x and y axis, determined from the Pagano solution in contact loading of an orthotropic material with $E_x/E_y = 5.10$. Contact zone size and pressure distribution are taken from Willis contour integration. Center of the contact zone is at $x = y = 15$ mm.

6. Discussion

The major point of the present work is to show that detailed stress and strain distributions in contact loading of orthotropic materials are easily obtained by using the numerical contour integration approach of Willis (1966), to determine the size and shape of the contact area and pressure distribution, and then using these values to determine the transverse loading that is needed for the approach of Pagano (1970) and Srinivas and Rao (1970). The accuracy of the solution can be assessed in part by comparison with known solutions such as for transversely isotropic materials and the depth of indentation for orthotropic materials, and in part by comparing the calculated surface displacement with the indentor profile. The examples shown indicate that good accuracy is achieved.

In the solution for contact of orthotropic materials shown in Figs. 5, 8, and 9, it is interesting to note that the ratio of the axes of the elliptical contact area are not a strong function of the orthotropic material properties. However the strains shown in Fig. 9 are significantly different in the x and y directions, and the stresses (not shown) would show an even greater difference.

The use of a rigid spherical indentor in the example problems was employed so as to focus on the essential steps in the approach. As is well known and discussed in Johnson (1985), for example, it is straightforward to include a deformable orthotropic indentor, by simply including the deformation of the indentor in Eq. (25). Further, the Willis solution is in principle applicable to general anisotropic materials, where the angle between the contact ellipse and the x, y coordinate system becomes an additional unknown. This angle could presumably be found by a root finding method similar to that used here to find the ratio of the axes of the contact area. However the Pagano and Srinivas and Rao solution only holds for orthotropic materials, so that other means, such as finite element analysis, would need to be used to determine the stress distributions.

It is likely that the procedures displayed above will be useful to obtain approximate solutions for more general geometries, such as contact loading of laminated materials with finite dimensions. For example, Swanson and Kim (2003) used an empirical modification of the theoretical pressure distribution obtained

from Chen (1969), to examine the effects of contact loading in orthotropic sandwich beams. This was accomplished by using the modified pressure distribution in a 2-D version of the Pagano analysis, and then minimizing the error between calculated surface displacement and indentor profile. The advantage is that one can start with a thick beam (or plate) where the half-space analysis would be expected to give good accuracy, and then systematically modify the geometry to be more specific to the actual finite thickness structure of interest.

7. Summary and conclusions

The problem of contact loading of an orthotropic half-space is examined. It is seen that a procedure outlined by Willis that uses numerical contour integration can be readily employed, along with iteration, to determine several features of the contact analysis, such as the size of the elliptical contact area, the contact pressure distribution, and the indentation depth. Example calculations were shown to compare with previous results for transversely isotropic materials, and the results show that good accuracy is achieved. New results are presented for orthotropic materials. The contact area and contact pressure distribution are then used with a solution for surface pressure loading of an orthotropic material by Pagano and Srinivas and Rao to determine the stress and strain fields throughout the region. The results show that for orthotropic materials under contact loading by a spherical indentor, the contact area is elliptical but differs from circular by only a modest amount, and that the stress and strain distributions differ significantly from that for isotropic or transversely isotropic materials.

References

Chao, C.C., Tu, C.Y., 1999. Three-dimensional contact dynamics of laminated plates: Part 1. Normal impact. Compos. Part B: Eng. 30, 9–22.

Chen, W.T., 1969. Stresses in some anisotropic materials due to indentation and sliding. Int. J. Solids Struct. 5, 191–214.

Dahan, M., Zarka, J., 1977. Elastic contact between a sphere and a semi infinite transversely isotropic body. Int. J. Solids Struct. 13, 229–238.

Green, A.E., Zerna, W., 1954. Theoretical Elasticity. Oxford University Press, Oxford.

Johnson, K.L., 1985. Contact Mechanics. Cambridge University Press, Cambridge.

Leknitskii, S.G., 1963. Theory of Elasticity of an Anisotropic Elastic Body. Holden-Day, San Francisco.

Miller, G.R., 1986. A green's function solution for plane anisotropic contact problems. J. Appl. Mech. 53, 386–389.

Pagano, N.J., 1970. Exact solutions for rectangular bidirectional composites and sandwich plates. J. Compos. Mater. 4, 20–34.

Shi, D., Lin, Y., Ovaert, T.C., 2003. Indentation of an orthotropic half-space by a rigid ellipsoidal indenter. J. Tribol. 125, 223–231.

Srinivas, S., Rao, A.K., 1970. Bending, vibration and buckling of simply supported thick orthotropic rectangular plates and laminates. Int. J. Solids Struct. 6, 1463–1481.

Sveklo, V.A., 1964. Boussinesq type problems for the anisotropic half-space. PMM 28, 908–913.

Swanson, S.R., 1997. Introduction to Design and Analysis with Advanced Composite Materials. Prentice-Hall, Englewood Cliffs, NJ.

Swanson, S.R., 2000. Response of orthotropic sandwich plates to concentrated loading. J. Sandwich Struct. Mater. 2, 270–287.

Swanson, S.R., Kim, J., 2003. Design of sandwich structures under contact loading. Compos. Struct. 59, 403–413.

Tan, T.M., Sun, C.T., 1985. Use of statical indentation laws in the impact analysis of laminated composite plates. J. Appl. Mech. 5, 6–12.

Turner, J.R., 1966. Contact on a transversely isotropic half-space, or between two transversely isotropic bodies. Int. J. Solids Struct. 16, 409–419.

Willis, J.R., 1966. Hertzian contact of anisotropic bodies. J. Mech. Phys. Solids 14, 163–176.

Wu, E., Yen, C.S., 1994. The contact behavior between laminated composite plates and rigid spheres. J. Appl. Mech. 61, 60–66.

Yang, S.H., Sun, C.T., 1982. Indentation law for composite laminates. In: Daniel, I.M. (Ed.), Composite Materials: Testing and Design, 6th Conference. In: ASTM STP 787. pp. 425–449.